ELSEVIER

Journal of Chromatography A, 897 (2000) 65–80

JOURNAL OF CHROMATOGRAPHY A

www.elsevier.com/locate/chroma

Protein adsorption on novel acrylamido-based polymeric ion-exchangers
I. Morphology and equilibrium adsorption

Alan K. Hunter, Giorgio Carta*

Department of Chemical Engineering, University of Virginia, Charlottesville, VA 22903-2442, USA

Received 26 January 2000; received in revised form 30 May 2000; accepted 17 July 2000

Abstract

The protein uptake equilibrium and particle morphology are determined for novel polymeric ion-exchange media based on acrylamido monomers with a high density of functional groups and a variety of morphological characteristics. The study considers two anion-exchangers and a cation-exchanger. Physical properties determined experimentally include particle density, ion-exchange capacity, particle size distribution, and equilibrium isotherms for model proteins. The pore structure was evaluated using size exclusion chromatography with neutral probe molecules and transmission electron microscopy. For the anion-exchangers, two types of structures were inferred. The first is comprised of particles that contain a low-density gel supported by denser polymer aggregates. This material had a very low size-exclusion limit for neutral probes, but exhibited an extremely high and reversible protein adsorption capacity (280–290 mg BSA/ml). The second structure is comprised of particles with large, open macropores. While the size-exclusion limit was very high, the protein adsorption capacity was low (60 mg BSA/ml). Moreover, the adsorption was nearly irreversible. The physical structure of the cation-exchanger appeared to be intermediate between those of the anion-exchangers, containing both large pores and smaller pores yielding an intermediate, but reversible, protein uptake capacity (120–130 mg αCHY/ml). The different behavior of these materials with regards to protein adsorption correlates well with their physical structure. For these ion-exchangers, high protein adsorption capacities are attained when a low-density polymer gel with a high concentration of functional groups is present.

Keywords: Ion exchangers; Adsorption; Polymeric gels; Stationary phases, LC; Proteins

1. Introduction

The development of stationary phases for the recovery and separation of biological macromolecules by ion-exchange continues to attract considerable interest [1]. In particular, there is a growing interest in stationary phases that are sufficiently rigid to permit operation at elevated flow-rates of the mobile phase in order to increase productivity [1,2]. To optimally design such a material, one is normally forced to find a balance between high capacity, rapid kinetics, and mechanical strength. Traditionally, the first is attained with gel-type structures; the second is obtained with wide, open-pore structures; and the third is obtained with rigid matrices, such as silica or highly cross-linked hydrophobic polymers. Two

*Corresponding author. Tel.: +1-804-924-6281; fax: +1-804-982-2658.

E-mail address: gc@virginia.edu (G. Carta).

0021-9673/00/$ – see front matter
PII: S0021-9673(00)00864-5

additional, important considerations are: (a) chemical stability with regard to leakage of functional groups and ability to withstand alkaline sanitizing conditions and (b) inertness with regard to non-specific binding.

Recent advances in this area include the so-called ''perfusive'' matrices, where transport rates can be enhanced by intraparticle convection [3–6], and gel–composite media, where mechanical strength and high capacity are obtained by incorporating a functionalized hydrogel in the pores of a rigid matrix [7–10]. Perfusive particles based on coated polystyrene matrices and gel–composite media based on polyacrylamide-gel–silica composites are commercially available [11,12]. Polymeric stationary phases that are based entirely on hydrophilic monomers but that have sufficient rigidity to withstand high mobile-phase velocities are a further alternative. For example, a variety of acrylamido-based monomers possessing either anion- or cation-exchange functionalities are available. Such monomers can be polymerized in the presence of porogens to yield particles with a high density of functional groups and with different morphological characteristics. Since no post-polymerization coating or derivatization is needed, these particles can in principle have an extremely high chemical stability. Media of this type have recently been developed by Bio-Rad Laboratories, Inc. (Hercules, CA, USA) and are referred to in this manuscript as ''BRX ion-exchange media''. These materials have been reported to be stable in 1 *M* NaOH virtually indefinitely and to exhibit very high dynamic-binding capacities even at velocities of 600–1200 cm/h [13].

In spite of commercial advances, the design of optimized particles remains largely empirical. This is due to the fact that the relationship between particle morphology, adsorption equilibrium, and intraparticle transport rates is not known with sufficient certainty. It has proved difficult to predict static adsorption capacities and diffusion rates especially in gel-type particles and few studies have provided a complete characterization of both morphology and adsorptive properties. Thus, in this work we have conducted a systematic investigation of morphological and adsorptive characteristics of BRX ion-exchange media. The goal is to develop a basic understanding of how these particles function in order to form a basis for their rational design.

The study considers two anion-exchangers having the same basic quaternary ammonium ion functionality but different morphology and charge density as well as a cation-exchanger with sulfopropyl functionality. The properties of the anion-exchangers can, of course, be compared directly since the surface chemistry is the same. However, while some of the properties are strongly dependent on surface chemistry (e.g., protein binding), others are expected to depend primarily on the physical morphology. For example, size exclusion characteristics for neutral solutes and pore diffusion mechanisms are not expected to depend on surface chemistry. Thus, it is possible to draw certain useful comparisons between anion- and cation-exchangers.

Physical and morphological properties studied include appearance under scanning electron microscope (SEM) and transmission electron microscope (TEM) analyses, apparent and skeletal densities, ion-exchange capacity, particle size, size exclusion chromatography (SEC) with neutral probe molecules, and protein adsorption equilibria. Adsorption rates in batch and shallow bed contactors and column breakthrough curves were also determined and are reported in Part II of this work.

2. Materials

BRX-Q and BRX-S stationary phases were obtained from Bio-Rad Laboratories, Inc. (Hercules, CA, USA). According to the manufacturer, these phases are based on water-soluble, hydrophilic acrylamido and vinylic monomers that are polymerized in the presence of porogens to yield spherical particles with varying degrees of porosity and rigidity. Ion-exchange functionality is introduced by adding an ''ionogenic monomer'', which contains the desired ion-exchange functionality, to the polymerization mixture. The ligand monomer becomes incorporated in the final polymerized product. Hence, no post-polymerization derivatization is needed [15]. BRX-Q is a strong anion-exchanger with a quaternary ammonium ion functionality. BRX-S is a strong cation-exchanger with a sulphopropyl functionality. A third sample, which will be referred to as BRX-QP, was also obtained from Bio-Rad and studied for comparison purposes. According to the manufac-

turer, this material is based on the same chemistry of BRX-Q, but starting with only 40% (w/w) of the amount of ionogenic monomer in the initial monomer mixture compared to the original BRX-Q media.

All of the media samples were pretreated in a gravity-fed column by washing with alternating cycles of 500 m*M* NaCl and dilute buffer solutions. A clear effluent with no detectable absorbance in the UV spectrum was obtained following the first few cycles. All experiments were conducted in 50 m*M* Tris–HCl buffer at pH 8.5 for the anion-exchangers and in 10 m*M* Na_2HPO_4 buffer at pH 6.5 for the cation-exchanger at room temperature ($T=22\pm2$°C). Following pretreatment, the samples were stored under refrigeration in buffer.

Bovine serum albumin (BSA, Fraction V powder, Cat. No. A-6918) and α-chymotrypsinogen (αCHY, Type II, Cat. No. C-4879) were obtained from Sigma Chemical Co. (St. Louis, MO, USA) and used without further purification. The purity stated by the manufacturer was >98% for both proteins. Molecular weights and isoelectric points are M_r~65 000 and p*I*~5 for BSA and M_r~26 500 and p*I*~9.5 for αCHY [14]. Dextrans and polyethylene glycols for SEC experiments were obtained from Pharmacia (Piscataway, NJ, USA) and from Sigma. Chemicals for the preparation of embedding media for TEM imaging were from Electron Microscopy Sciences (Ft. Washington, PA, USA) and gold-labeled BSA was from Sigma (Cat. No. A-5179). Other chemicals were obtained from Sigma and from Fisher Scientific (Pittsburgh, PA, USA).

3. Methods

3.1. Particle densities

The media skeletal density, ρ_s, was determined by helium densitometry using a Coulter Omnisorb apparatus. The particle solid density, ρ_d, was obtained by packing the media in a glass column and determining the extraparticle void fraction from pressure drop measurements as described below. The column was then emptied and the dry weight of packing determined by drying the particles in an oven at 120°C. Total particle porosity, ϵ_{pt}, was calculated as $\epsilon_{pt}=1-\rho_d/\rho_s$. This porosity represents the contributions of all pores including both permanent pores and any gel-type porosity that may exist in the material. From microscopic visualization, we observed very little volume change for dry and hydrated particles. Hence, the wet particle density was calculated from the expression $\rho_{pw}=\epsilon_{pt}\rho_w+(1-\epsilon_{pt})\rho_s$, where ρ_w is the density of water.

3.2. Ion-exchange capacity

Direct acid or base titrations converting the media from the hydrogen or hydroxide form to a corresponding salt determined the ion-exchange capacity. This method was checked for the anion-exchangers by starting with the chloride form and equilibrating the media with an excess of 0.1 *M* NaOH. The chloride concentration in the supernatant was then determined by the Volhard titration method. Results in close agreement with those of direct titrations were obtained. Capacities were calculated by material balance on a dry-basis and converted to a particle-volume basis using the particle solid density.

3.3. Particle size distribution

Particle size distributions were obtained from microphotographs of hydrated media at 100× magnification using a calibrated scale. The particles are nearly spherical. Mean particle diameters calculated from this procedure were in good agreement with values obtained by the manufacturer based on a Horbia LA-500 particle size analyzer [15].

3.4. Electron microscopy

Both SEM and TEM images were obtained. Bio-Rad Laboratories provided SEM images obtained by drying and gold-coating the samples. For TEM analyses, the particles were first embedded in a resin matrix using procedures similar to those used for imaging biological specimens. This should preserve, at least in part, the hydrated structure of the media [16]. The particles were dehydrated by first treating them with a 50:50 (v/v) ethanol–water mixture and then with four washes of anhydrous ethanol. A Spurr's embedding resin mixture, containing 10 g of vinyl cyclohexene dioxide, 4 g of diglycidyl polypropylene glycol ether, 26 g of nonenyl succinic

anhydride, and 0.3 g of dimethyl aminoethanol, was then prepared. The dehydrated particles were first infiltrated with a 50:50 (v/v) ethanol–Spurr's resin mixture and then washed with pure Spurr's resin mixture four times. The samples were cured overnight at 70°C. After curing, the embedded samples were cut into 80-nm sections using a Leica Ultracut UCT microtome equipped with a DiaTOME diamond knife (45°). The sections were collected on copper electron microscopy grids (200–300 mesh) and stained with a 2% aqueous uranyl acetate–lead citrate solution for 20 min. TEM analyses were then performed with a JEOL 100 CX electron microscope. Sections of embedded BRX-Q media were also exposed to a colloidal gold-labeled BSA suspension (10-nm gold particles). For this purpose, the sections were treated with Tris buffer, washed with a 0.2% Tween 20 solution in Tris, exposed to a 1:25 AuBSA suspension–Tris buffer for 3 h, and then rinsed with buffer. The sections were than stained with a uranyl acetate–lead citrate solution for 20 min.

3.5. Size exclusion chromatography

SEC experiments were conducted using Dextran T-fractions (Pharmacia), polyethylene glycols (PEG), and glucose as inert probes. Although the relationship between retention volume in SEC and pore size is complicated and it is sometimes impossible to interpret the results unambiguously in terms of a unique pore-size distribution [17], these experiments can still provide useful information on the fraction of particle volume accessible by different probe molecules. All SEC experiments were carried out in 50 m*M* Tris buffer at pH 8.5 for the anion-exchangers and in 10 m*M* Na_2HPO_4 buffer at pH 6.5 for the cation-exchanger at room temperature. The media samples were slurry packed in 0.5-cm I.D., glass columns (Mod. HR 5/15, Pharmacia, Piscataway, NJ, USA) to a depth of 9–10 cm. The mobile phase was supplied with a Pharmacia Mod. P-500 syringe pump at flow-rates of 0.25 ml/min. Samples (0.05 ml, 2.5 mg/ml) were injected with a Rheodyne six-port valve and detected with a Waters Mod. R401 differential refractive index detector. The detector output was collected on a computer and analyzed with a spreadsheet to determine the first statistical moment. Blank runs, conducted without the packing and pushing the inlet and outlet frits of the column against each other were used to make a correction for the extra-column contribution to the first moment. The distribution coefficient was calculated from:

$$K_D = \frac{\frac{V_R}{V_C} - \epsilon_b}{(1 - \epsilon_b)} \quad (1)$$

where V_R is the elution volume, V_C is the bed volume and ϵ_b is the extraparticle void fraction. Note that K_D is based on the entire particle volume. This definition was used since the particles are heterogeneous. Thus, $K_D = 0$ for a solute that is completely excluded while $K_D = \epsilon_{pt}$ for a solute that gains access to the entire particle porosity. Pressure drop curves were obtained for these columns using a mercury-filled, U-tube manometer in order to estimate ϵ_b. The pressure drop curves were linear with mobile phase velocity. Accordingly, the Kozeny equation [18] was used to calculate ϵ_b from:

$$\frac{\Delta P}{L} = 150 \frac{\eta u}{\bar{d}_p^2} \frac{(1 - \epsilon_b)^2}{\epsilon_b^3} \quad (2)$$

where η and u are the mobile phase viscosity and superficial velocity and $\bar{d}_p$ is the average particle diameter. An equation taking into account the particle size distribution is also available [19]. However, its use does not yield significantly different results, except when the distribution is highly skewed. As a possible alternative method to determine ϵ_b, the use of large probe molecules for SEC experiments was considered. Although this approach can be adequate for relatively small pore media, it was rejected in our case because of difficulties in finding a neutral probe which is sufficiently large to be excluded from the very large pores of some of the materials studied.

3.6. Adsorption isotherms

Adsorption isotherms were obtained for BSA on BRX-Q and BRX-QP and for αCHY on BRX-S by a batch equilibration method. Small samples of hydrated media ($M_w \sim 0.025$ g) were placed in vials with a volume ($V = 6$ ml) of a solution containing a known initial protein concentration, C_0. The vials were sealed and rotated end-to-end at a few rpm and

the supernatant analyzed for protein content with a UV spectrophotomer (Beckman, Mod. DU50). After establishment of equilibrium (shown by the absence of any further change in protein concentration in the supernatant) the uptake of protein by the media was calculated from:

$$q' = \frac{V}{M_w}(C_0 - C^*) \quad (3)$$

where C^* is the final protein concentration. Six hours were found sufficient to attain equilibrium in our experiments. The media sample dry weight and the known particle solid density were then used to convert q' to an uptake q expressed in terms of hydrated particle volume. Equilibrium experiments were repeated at different salt concentrations by adding NaCl to the corresponding buffer.

4. Results and discussion

A summary of physical properties for the particles studied is given in Table 1. Under microscopic examination, the particles are translucent. In aqueous buffers they settle slowly indicating a low solid content. On a volume basis, the total water content is in excess of 80% (v/v). As shown by the distribution coefficients for the smallest and largest SEC probe molecules used, the effective ''pore sizes'' of the different materials are dramatically different. The particle size distributions (PSD) were fairly symmetrical and narrow as indicated by the relatively small value of the standard deviation, σ_p. The PSD was somewhat broader for the BRX-S media, which has a smaller average size. The ion-exchange capacities of the commercial materials are very high on a dry-weight basis. In fact, the q_0'-values for the BRX-Q and BRX-QP media are in the same ratio as the ratio of ionogenic monomer used in the polymerization. A ''sorption efficiency'' (mg of protein bound per μeq of ion-exchange capacity) was also calculated as suggested by Boschetti [1] as a measure of the accessibility of the charged functional groups. The values obtained for these materials can be compared with those for several commercial ion-exchangers given in Ref. [1].

SEM images of the BRX-Q and BRX-S particles are shown in Fig. 1. Both particles have a ''spongy'' appearance, which is suggestive of wide, open pores. SEM images of sections of these particles showed that this appearance persists in the interior of the particles as well. However, it should be recognized that these images reflect only the dry structure. Although they cannot provide information on structural elements that depend on hydration and that collapse on drying, the SEM images reveal that these particles have a highly heterogeneous structure. This information is complemented by the TEM images

Table 1
Properties of the materials

Property	Units	BRX-Q	BRX-QP	BRX-S
ρ_s	g solid/ml solid	1.30	1.30[d]	1.50
ρ_d	g dry solid/ml wet particle	0.24	0.18	0.21
ρ_{pw}	g wet particle/ml wet particle	1.06	1.04	1.07
ϵ_{pt}[a]	–	0.81	0.88	0.87
K_D (glucose)[b]	–	0.73	0.80	0.76
K_D (Dextran T-500)[b]	–	~0.01	0.50	0.42
d_p	μm	89	98	63[c]
σ_p	μm	18	25	21[c]
q_O'	μeq/g dry particle	1100	440	990
q_O	μeq/ml wet particle	270	80	210
Sorption efficiency	mg/μeq	1.00[e]	0.80[e]	0.60[f]

[a] Particle porosity determined from skeletal and apparent densities.
[b] Distribution coefficient determined by SEC.
[c] Measured by Bio-Rad Laboratories.
[d] Assumed.
[e] Based on protein uptake capacity for BSA.
[f] Based on protein uptake capacity for αCHY.

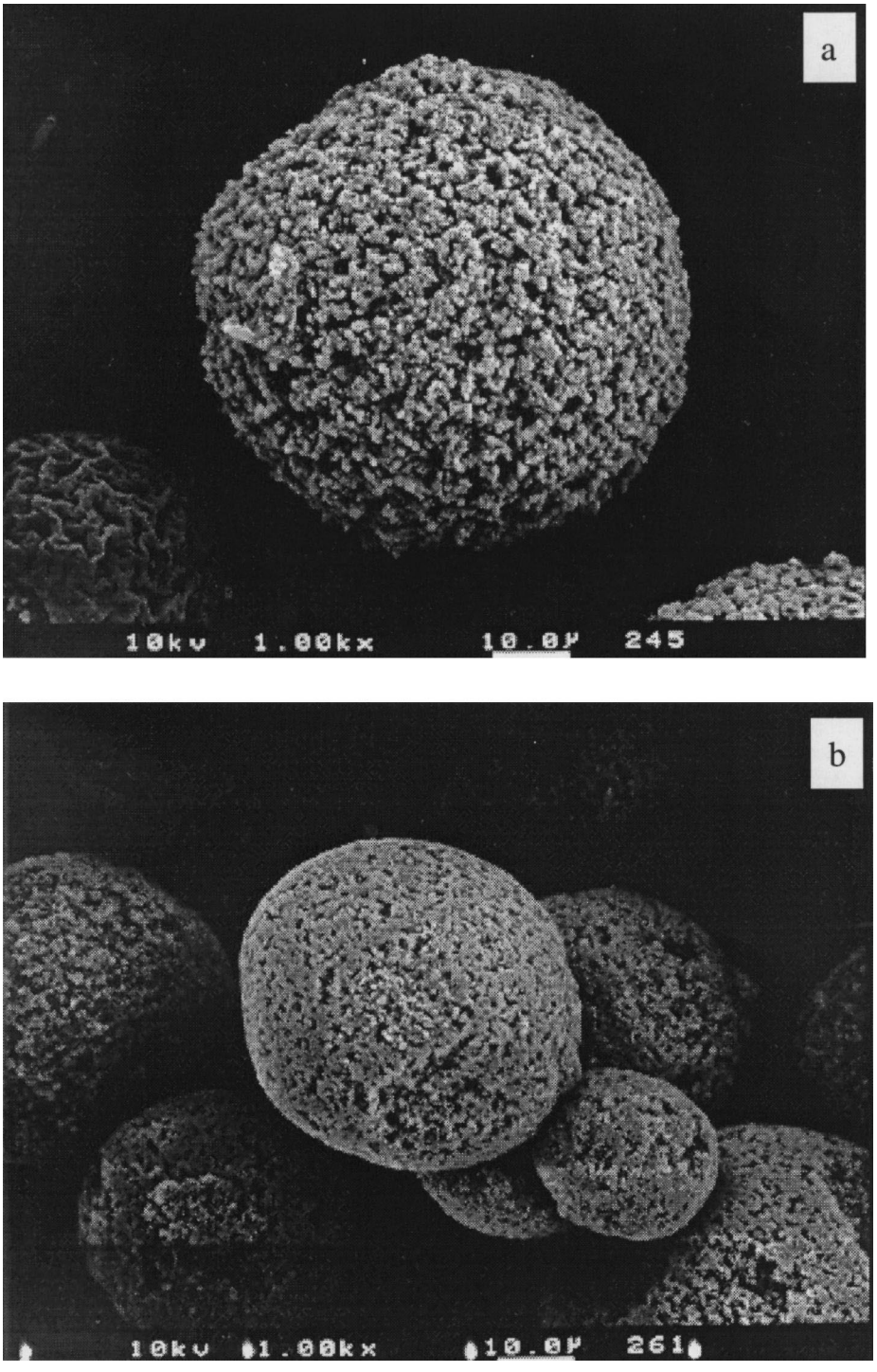

Fig. 1. Scanning electron micrographs of (a) dry BRX-Q and (b) BRX-S particles.

shown in Fig. 2. Distinctly different features are visible. In both images the lighter background represents the embedding resin which is not stained by uranyl acetate. The darker areas represent the solid backbone of the particles. In the case of BRX-S (Fig. 2b), the particles comprise denser areas that appear to be randomly distributed. The denser aggregates are seen to define an open macropore network, with some pores in the range 0.7–1.5 μm. However, many small pores also exist dispersed in the solid matrix. Connected areas of solid aggregates can be seen extending from the surface of the particle (top of image) toward the center. In the case of BRX-Q (Fig. 2a), the particles also appear to contain denser aggregates, which are larger on average than in the BRX-S particles. However, these denser aggregates do not seem to define open pores, since uranyl acetate-stained material is visible virtually anywhere in the lighter areas surrounding the denser aggregates. We can exclude that these are artifacts resulting from sectioning, since there appears to be no preferential orientation and the same features were visible in all the BRX-Q particles examined. A TEM image of a AuBSA stained BRX-Q section is shown in Fig. 3. The colloidal gold is visible as small dots and indicates positively charged binding sites exposed in the sectioning process. As seen in Fig. 3, although the concentration of gold particles is greater in the denser aggregates, gold particles are also seen bound to the lighter areas. No gold particles were seen bound anywhere in the Spurr's resin outside the particles (see, for example, the bottom right corner of the image showing the particle boundary).

Thus, based on the complementary information provided by SEM and TEM images, we can conclude that the BRX-Q particles possess a heterogeneous distribution of polymer densities. They contain denser aggregates that provide mechanical strength, surrounded by a lighter phase, which collapses on drying. The former are evident in both SEM and

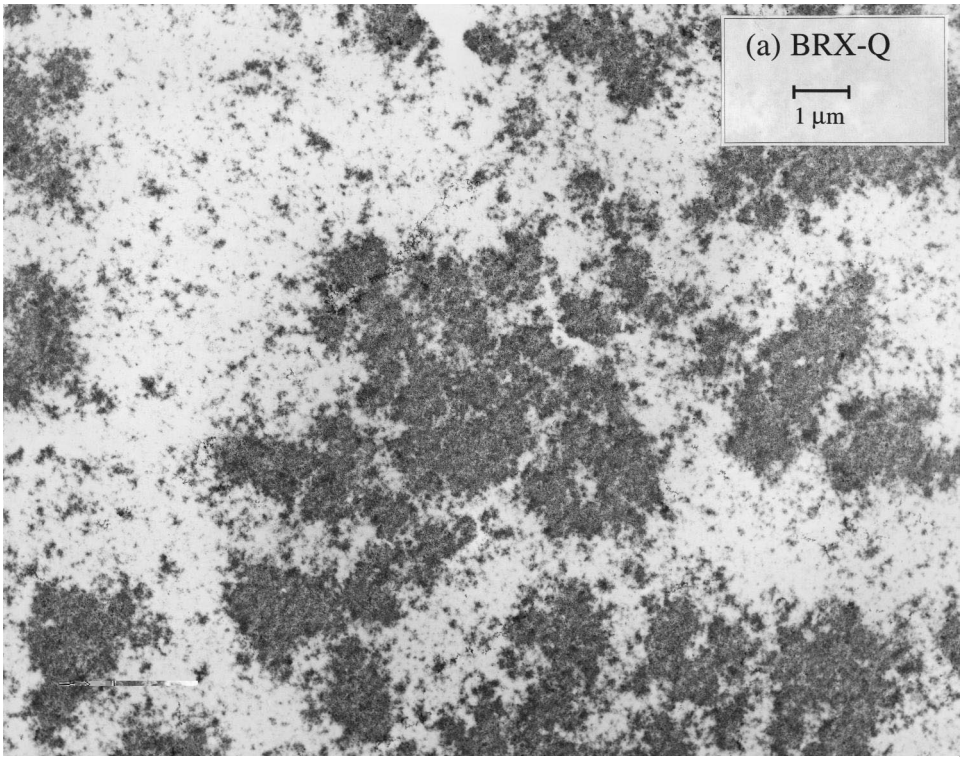

Fig. 2. Transmission electron micrographs of sections of particles embedded in Spurr's resin. Original magnification 5000×. (a) BRX-Q and (b) BRX-S.

Fig. 2. (*continued*).

TEM images, while the latter is evident only in TEM images. BRX-S, on the other hand, clearly contains a network of open pores as well as areas of smaller pores. In this case, both SEM and TEM images provide consistent views. This conclusion is further supported by the SEC results discussed below. As shown in Table 1, glucose ($M_r = 180$) gains access to a large fraction of the particle volume for both BRX-Q and BRX-S. However, Dextran T-500 ($M_r \sim$ 500 000) is essentially completely excluded from the BRX-Q particles while it still retains access to a substantial portion of BRX-S. We did not carry out extensive TEM analyses of the BRX-QP particles. However, these particles have a similar SEM appearance and are likely to contain a large fraction of open pores since the distribution coefficient for glucose is very large and a large fraction of the particle volume is accessible by Dextran T-500 (see Table 1).

SEC peaks for Dextran T-fractions and glucose are shown in Fig. 4 for BRX-Q, BRX-QP, and BRX-S. The data are shifted along the *x*-axis to account for the extracolumn retention volume obtained as discussed in Section 3. The Dextran T-fractions used have the following approximate average molecular masses: T-10 = 10 000, T-40 = 40 000, T-70 = 70 000, and T-500 = 500 000. PEGs with average molecular masses of 300, 400, 1450, and 8000 were also used, although for simplicity, the corresponding chromatographic peaks are not included in the figure. The pressure drop curves for these columns are shown in Fig. 5 along with their fit with Eq. (2). The calculated extraparticle void fractions for the BRX-Q, BRX-QP, and BRX-S columns were 0.33, 0.41, and 0.33, respectively. These values correspond to V_R/V_C for a probe completely excluded from the stationary phase. As seen in Fig. 4, the SEC behavior for the BRX-Q media (Fig. 4a) is very different. Dextran T-40 and larger probes elute with essentially the same retention volume, and this is very close to the extraparticle void volume. At the same time there

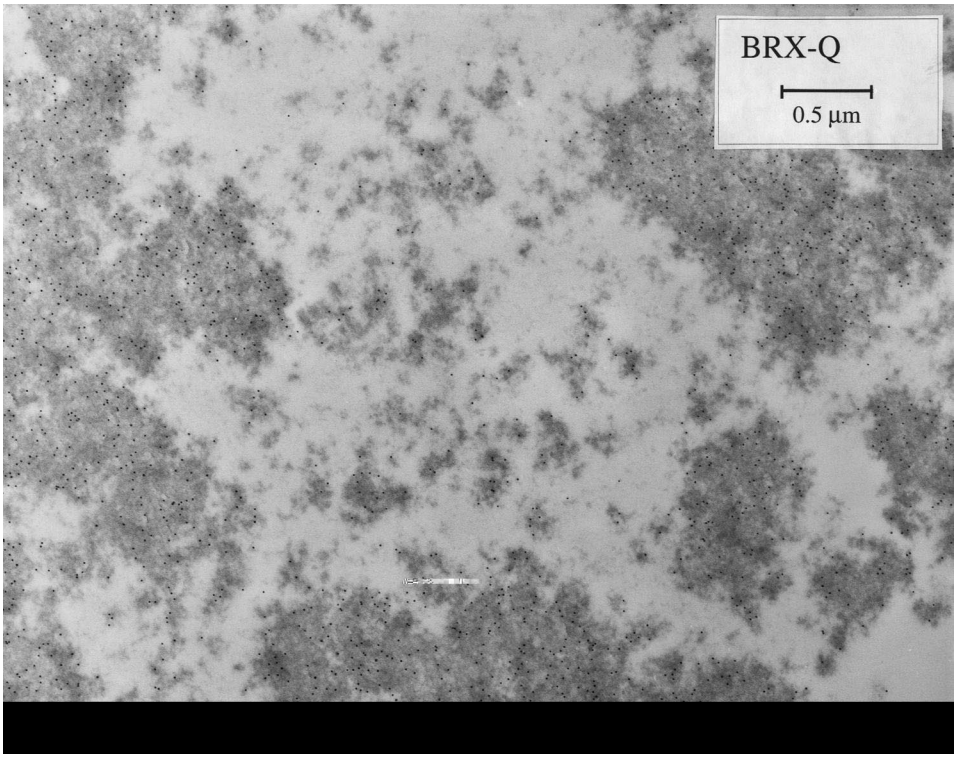

Fig. 3. Transmission electron micrographs of BRX-Q sections embedded in Spurr's resin and exposed to gold-labeled BSA. Original magnification 16 000×.

is a very high resolution between glucose and Dextran T-10. Conversely, for BRX-QP and BRX-S, even for the higher molecular mass dextrans there are very significant differences in retention volume. The separation between glucose and Dextran T-10 is much more limited in this case. It should be noted that the peak skewness observed with the higher molecular mass dextrans is largely due to extracolumn or sample effects. In fact, peaks of similar skewness were obtained in blank runs without the packing performed as discussed above. It should also be noted that although the linear polymers used as SEC probes are structurally different from proteins, the results can be related to those for globular molecules by correlating the K_D-values in terms of the molecules' viscosity radius, r_s [20]. Fig. 6 shows the results in this form. The viscosity radius was calculated from the following equations from Squire [20]:

$$\text{For dextrans:} \quad r_s = 0.028 \times M_r^{0.47} \tag{4}$$

$$\text{For PEGs:} \quad r_s = 0.025 \times M_r^{0.50} \tag{5}$$

The radius of glucose was taken as 0.36 nm [17]. The results in Fig. 6 show that BRX-Q has size-exclusion resolution capability for solutes with viscosity radius less than about 2 nm, while it nearly completely excludes neutral probes with radius greater than about 4 nm. BRX-QP and BRX-S, on the other hand, can accommodate even very large molecules.

Theoretical expressions for K_D are available for ideal materials. For media with macropores of radius r_{pore}, a cylindrical pore approximation is often used giving [21]:

$$K_D = \epsilon_p \left(1 - \frac{r_s}{r_{pore}}\right)^2 \tag{6}$$

where ϵ_p is the particle macroporosity. For materials that consist of a fibrous gel, on the other hand, we have [22,23]:

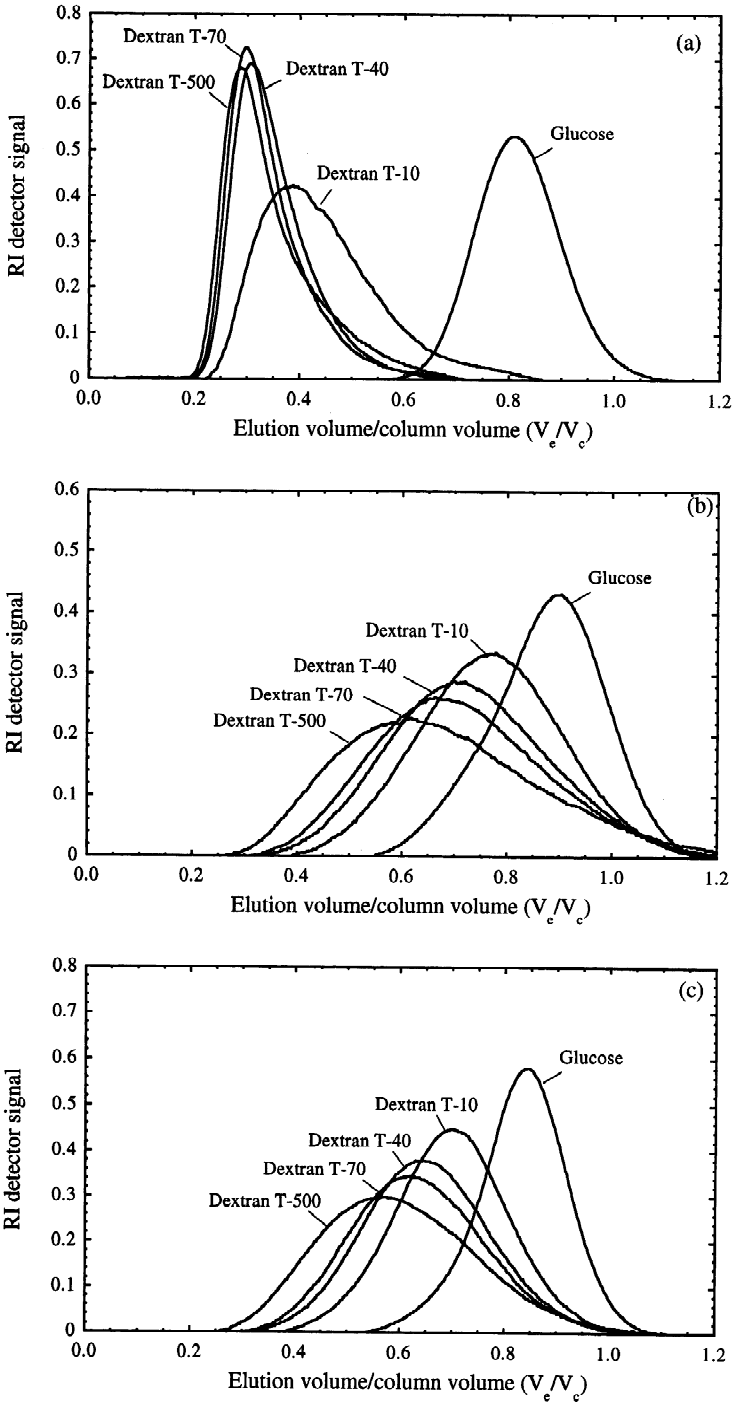

Fig. 4. Size exclusion chromatography peaks for glucose and Dextran T-fractions on (a) BRX-Q, (b) BRX-QP, and (c) BRX-S columns. Experimental conditions are noted in text.

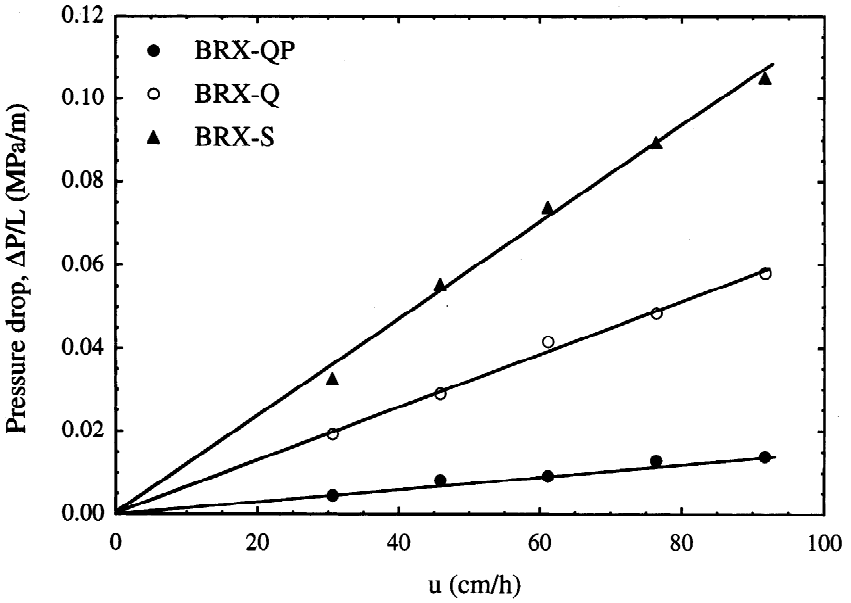

Fig. 5. Pressure drop curves for BRX-Q, BRX-QP, and BRX-S columns. Lines are based on Eq. (2).

$$K_D = \exp\left[-\phi\left(1+\frac{r_s}{r_f}\right)^2 \right] \quad (7)$$

where ϕ is the volume fraction of polymer in the gel and r_f is the fiber radius. However, an exact theoretical interpretation of our size exclusion curves in terms of either of these equations could not be obtained, likely because of the heterogeneous struc-

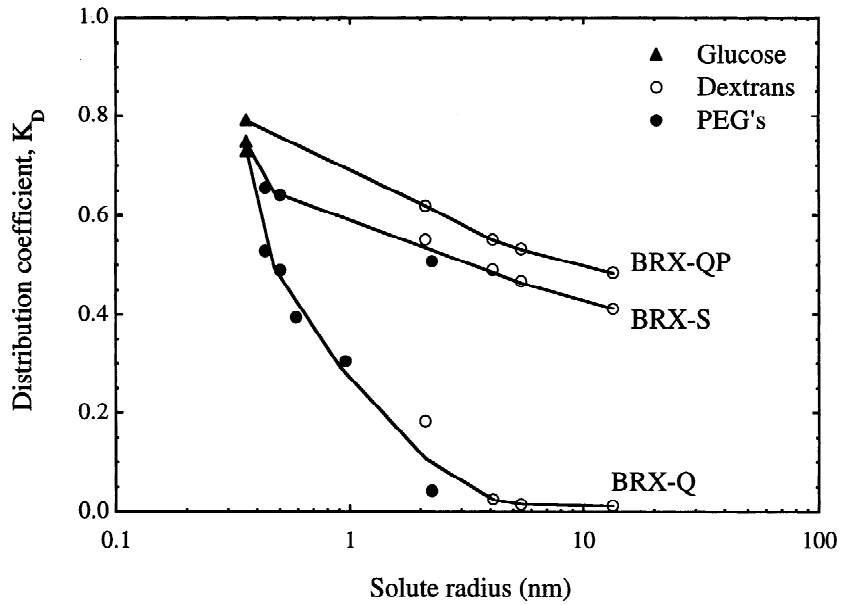

Fig. 6. Selectivity curve for BRX-Q, BRX-QP, and BRX-S using glucose, Dextran T-fractions, and polyethylene glycols. The solute radius is calculated according to Eqs. (4)–(5).

ture. It may be possible to assume a pore size distribution and fit the data accordingly. On the other hand, as discussed by Hagel et al. [17], it is difficult to do this unambiguously since different distributions can give the same fit. Nevertheless, we can conclude that BRX-Q must contain many small pores, while BRX-QP and BRX-S contain predominately large pores. To further elucidate this point, we injected mixtures of PEGs with 300 and 1450 molecular masses. The results, shown in Fig. 7, indicate that BRX-Q can resolve these mixtures while no resolution is detectable with either BRX-QP or BRX-S. To achieve this level of resolution, BRX-Q must contain a gel-porosity with ''pores'' 0.6–2 nm in size. The exact nature of this gel-porosity is not known. One possibility is that the space between the denser aggregates is filled with a crosslinked polymer gel phase (e.g., see Ref. [24]. Another possibility is that this space is filled with linear oligomers of the ionogenic monomer extending from the surface of the denser aggregates and forming a ''viscous'' phase. In either case, the properties of this phase determine the size exclusion characteristics of the matrix.

Adsorption isotherms for BSA on BRX-Q and BRX-QP and for αCHY on BRX-S are shown in Figs. 8–10. An extremely high uptake capacity of around 280 mg/ml is attained for BRX-Q at a concentration of 0 m*M* salt. For these conditions the isotherm is nearly rectangular and the efficiency of utilization of functional groups is approximately 1 mg/μeq. As the salt concentration is increased the isotherm becomes less steep. No BSA adsorption was detectable in 500 m*M* NaCl and >98% of adsorbed protein could be recovered at this salt concentration. Solid lines in Fig. 8 represent a description of the adsorption behavior in terms of the steric–mass–action (SMA) model of Brooks and Cramer [25]. The model is expressed by:

$$C = \frac{qC_I^z}{K[q_0 - (z+\sigma)q]^z} \tag{8}$$

where C_I is the counter-ion concentration, z is the protein characteristic charge, σ is a steric hindrance parameter, and K is the equilibrium constant for the exchange of the protein with the salt counter-ion. The parameter values were obtained from a nonlinear fit of the data and are summarized in Table 2. As seen in Fig. 8, the model provides a fit of the isotherm data that appears to be within the experimental accuracy when NaCl is added. However,

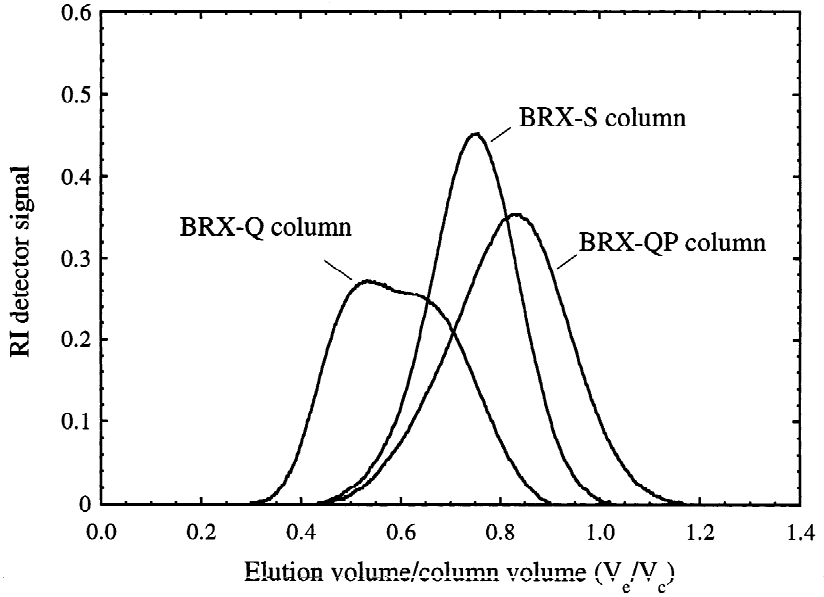

Fig. 7. Peaks obtained by injecting a 50:50 mixture of PEG 300 and PEG 1450.

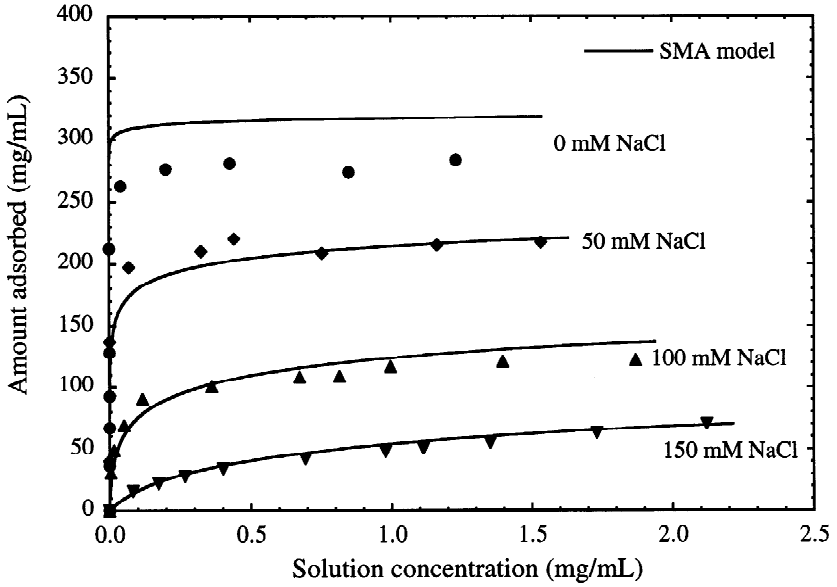

Fig. 8. Adsorption isotherm for BSA on BRX-Q in 50 m*M* Tris–HCl buffer at pH 8.5.

significant deviations occur in 0 m*M* NaCl where the capacity is predicted to be higher than observed experimentally.

Rather different results are obtained in the case of BRX-QP. As shown in Fig. 9, the maximum uptake capacity is limited to about 65 mg/ml. Moreover, BSA adsorption was nearly irreversible and the protein could not be desorbed even after exposing the media to 1 *M* NaCl. We can surmise that one of the reasons for these differences is the dramatic shift

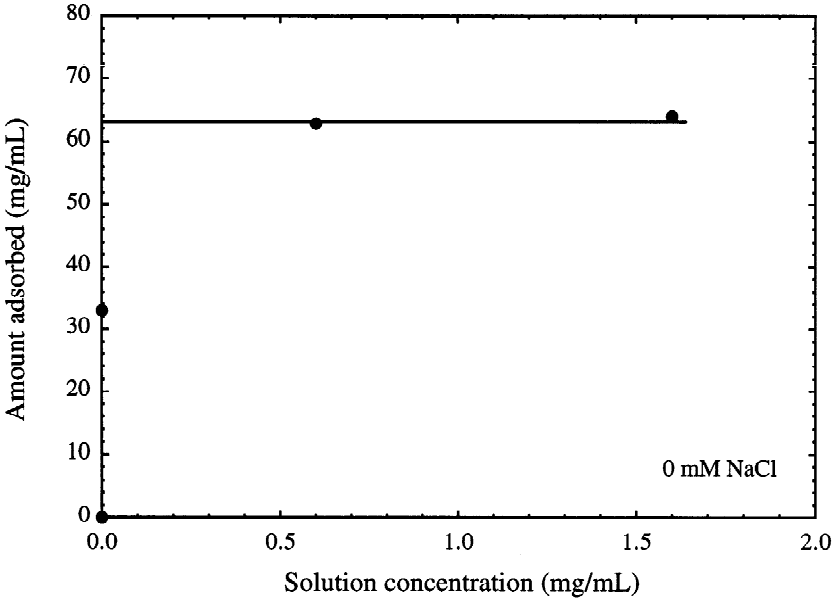

Fig. 9. Adsorption isotherm for BSA on BRX-QP in 50 m*M* Tris–HCl buffer at pH 8.5.

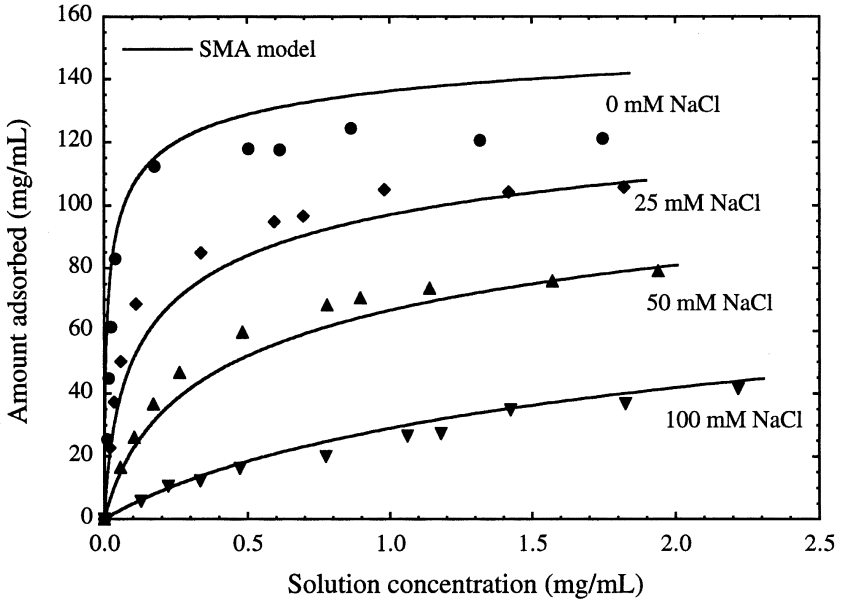

Fig. 10. Adsorption isotherm for αCHY on BRX-S in 10 m*M* Na_2HPO_4 buffer at pH 6.5.

in morphology that apparently occurs when the concentration of ionogenic groups is reduced. In the case of BRX-Q, if adsorption were limited to monolayer coverage of cylindrical pore surfaces, assuming a typical surface coverage for BSA of 1 mg/m^2, the adsorption capacity measured experimentally for this media would require a surface area, S_p, of 280 m^2/ml. An average pore size can be calculated from $r_{pore} = 2\epsilon_p/S_p$, where ϵ_p is the particle porosity [26]. Thus, assuming $\epsilon_p = 0.5$, we can calculate that this adsorption capacity would require pores 3.5 nm in radius. However, this is smaller than needed to accommodate the BSA molecule (hydrodynamic diameter~4 nm). Therefore, protein binding in BRX-Q must occur by interaction within the three-dimensional structure of a charged polymer-gel phase that exists within the media. This gel nearly completely excludes neutral probe molecules (e.g., Dextran T-40 which has essentially the same effective radius as BSA) but provides sites for a favorable ionic interaction with the negatively charged BSA at low or moderate salt concentrations. A behavior of this type has been previously observed for charged polyacrylamide gels immobilized in porous matrices [27]. In the case of BRX-QP, however, as shown by SEC results, the media comprises a network of large pores capable of accommodating molecules as large as Dextran T-500. As a result, protein adsorption occurs principally at the solid-fluid interface and is therefore likely limited to monolayer coverage. In this case, the experimental capacity of 63 mg/ml requires a surface area around 63 m^2/ml, or a pore size distribution with an average 16-nm radius. Such a distribution would appear to be consistent with the observed size exclusion curve for this material (Fig. 6).

Table 2
SMA equilibrium parameters

Material/protein	z	σ	K
BRX-Q/BSA[a]	9.0	45	2.6
BRX-S/αCHY[b]	3.5	27	8.0

[a] 50 m*M* Tris–HCl buffer, pH 8.5.
[b] 10 m*M* Na_2HPO_4 buffer, pH 6.5.

In the case of BRX-S (Fig. 10), the maximum adsorptive capacity for αCHY was around 120 mg/ml and was fully reversible. The data were adequately described by the SMA model, and fitted parameter values are given in Table 2. As in the case of BSA on BRX-Q, a substantial deviation occurs with no added salt, where lower than predicted capacities are

observed. Although an exact comparison of the absolute capacity values between the anion- and cation-exchange media is not possible since the protein and surface chemistries are different, we surmise that the qualitative behavior of BRX-S in this regard is inbetween that of BRX-Q and BRX-QP. In this case, the media contains large pores. However, it likely also contains gel-pores or micropores that provide a relatively large adsorption capacity. The sufficiently high density of ionogenic groups, indicated by the high q_0 value in this material, yields a highly hydrophilic environment that prevents the irreversible protein binding observed for BRX-QP.

5. Conclusions

We have examined morphological and adsorptive properties of recently developed stationary phases for protein chromatography based on charged acrylamido and vinyl monomers. Two anion-exchangers and a cation-exchanger were considered in order to explore both morphological and functional effects. For the anion-exchangers, two distinctly different morphologies were considered: one having a gel-type porosity dependent on hydration supported through a more rigid solid network; the other having distinct, open macropores. The anion-exchange matrix containing a gel-type porosity had SEC resolution capability for molecules with effective radii of less than 1 nm. The surprising result is that this matrix had an extraordinarily high BSA binding capacity while nearly completely excluding neutral probe molecules with radii greater than about 4 nm. This high capacity can be ascribed to a favorable binding environment in the gel structure that exists in these particles. Reduction in the concentration of ionogenic groups in the polymerization mixture lead to a particle containing predominately a macroporosity. The adsorption capacity was very low in this case and was likely to be limited by the available macropore surface area. An intermediate result was obtained with a cation-exchange matrix that contained macropores but still likely retained sufficient microporosity or a gel porosity to attain reasonably high adsorption capacities.

Finally, it is clear that considerable flexibility exists in the design of polymeric matrices based on acrylamido monomers. This flexibility can be exploited to define matrices that have different functionalities and morphologies, high chemical stability, high capacity, and sufficient mechanical strength for column operation. What remains to be seen is how the different morphologies influence mass transfer rates. This is dealt with in Part II of this work.

6. Nomenclature

C	Protein concentration in solution (mg/ml)
C_I	Counterion solution concentration (mol/l)
C_0	Initial protein concentration in solution (mg/ml)
C^*	Equilibrium protein concentration in solution (mg/ml)
$\bar{d}_p$	Average particle size (μm)
K	Equilibrium constant in SMA model
K_D	Distribution coefficient in SEC based on particle volume
L	Bed length (cm)
M_w	Mass of wet particles (g)
P	Pressure (Pa)
q	Protein concentration in particle (mg/ml)
q'	Protein concentration in particle (mg/g)
q_O	Ion-exchange capacity (μeq/ml)
q'_O	Ion-exchange capacity (μeq/g)
r_f	Fiber radius (nm)
r_{pore}	Pore radius (nm)
r_s	Molecule radius based on intrinsic viscosity (nm)
S_p	Surface area (m^2/ml)
u	Mobile phase superficial velocity (cm/s)
V	Solution volume (ml)
V_C	Column volume (ml)
V_e	Effluent volume (ml)
V_R	Retention volume based on first moment of peak (ml)
z	Effective charge
ϵ_b	Extraparticle void fraction
ϵ_p	Particle macroporosity
ϵ_{pt}	Total porosity of particle including gel-pores
ϕ	Volume fraction of polymer in gel
η	Viscosity (Pa/s)
ρ_d	Particle solid density (g/ml)
ρ_{pw}	Particle wet density (g/ml)

ρ_s Skeletal density (g/ml)
σ Steric hindrance parameter in SMA model
σ_p Standard deviation of particle size distribution (μm)

Acknowledgements

This research was supported by Bio-Rad Laboratories, Inc. and by NSF Grant No. CTS-9709670.

References

[1] E. Boschetti, J. Chromatogr. A 658 (1994) 207.
[2] H. Chen, Cs. Horváth, J. Chromatogr. A 705 (1995) 3.
[3] A.E. Rodrigues, L. Zuping, J.M. Loureiro, Chem. Eng. Sci. 46 (1991) 2765.
[4] G. Carta, M.E. Gregory, D.J. Kirwan, H.A. Massaldi, Sep. Technol. 2 (1992) 62.
[5] A.I. Liapis, M.A. McCoy, J. Chromatogr. 599 (1992) 87.
[6] D.D. Frey, E. Schweinheim, Cs. Horváth, Biotechnol. Progr. 9 (1993) 273.
[7] M.A. Fernandez, G. Carta, J. Chromatogr. A 746 (1996) 169.
[8] L.E. Weaver Jr., G. Carta, Biotechnol. Progr. 12 (1996) 342.
[9] A.E. Rodrigues, J.C. Lopes, C. Chenou, R. de la Vega, J. Chromatogr. B 664 (1995) 233.
[10] P.R. Wight, E.J. Muzzio, B.J. Glasser, Biotechnol. Progr. 14 (1998) 913.
[11] M. McCoy, K. Kalghatgi, F.E. Regnier, N. Afeyan, J. Chromatogr. A 743 (1996) 221.
[12] J. Horvath, E. Boschetti, L. Guerrier, N. Cooke, J. Chromatogr. A 679 (1994) 11.
[13] J.-L. Liao, H. Chen, L. Cummings, S. Franklin, R. Frost, W.-K. Lam, L. Olech, C. Ordunez, K. Talmadge, T. Tisch, in: PREP'99, San Francisco, CA, USA, 1999, Paper presented.
[14] P.G. Righetti, T. Caravaggio, J. Chromatogr. 127 (1976) 1.
[15] J.-L. Liao. Personal communication, 1999.
[16] G.A. Meeks, Practical Electron Microscopy For Biologists, 2nd ed, Wiley, New York, 1976.
[17] L. Hagel, M. Östberg, T. Andersson, J. Chromatogr. A 743 (1996) 33.
[18] R.B. Bird, W.E. Stewart, E.N. Lightfoot, Transport Phenomena, Wiley, New York, 1960.
[19] J.N. Tilton, Fluid and particle dynamics, in: D.W. Green (Ed.), Perry's Chemical Engineers Handbook, 7th ed, McGraw-Hill, New York, 1997, Section 6.
[20] P.G. Squire, J. Chromatogr. 210 (1981) 433.
[21] W.W. Yau, J.J. Kirkland, D.D. Bly, Modern Size Exclusion Liquid Chromatography, Wiley, New York, 1979.
[22] A.G. Ogston, Trans. Faraday Soc. 54 (1958) 1754.
[23] T.C. Laurent, Biochim. Biophys. Acta 136 (1967) 199.
[24] V. Kapur, J.C. Charkoudian, S.B. Kessler, J.L. Anderson, Ind. Eng. Chem. Res. 35 (1996) 3179.
[25] C.A. Brooks, S.M. Cramer, AIChE J. 38 (1992) 1969.
[26] G.F. Froment, K.B. Bischoff, Chemical Reactor Analysis and Design, Wiley, New York, 1979.
[27] D. Farnan, D.D. Frey, Cs. Horváth, Biotechnol. Progr. 13 (1997) 429.